 doi:10.20944/preprints201808.0145.v1

A new all-solid-state lithium-ion battery working without a separator in an electrolyte

Seonggyu Cho[a,b] , Shinho Kim[a], Wonho Kim[b], Seok Kim[b] Sungsook Ahn[a*]

[a] Secondary Battery R&D Center, DRB Holdings Co.,
Pusan, 46329, South Korea
[b] Department of Chemical and Biochemical Engineering, Pusan National University,
Pusan, 46241, South Korea

Corresponding
*E-mail: sungsookahn@yahoo.com

Keywords: Secondary lithium ion battery; All-solid-state battery**;** Solid polymer electrolyte**;** Succinonitrile (SN)**;** lithium(trifluoromethanesulfonyl)imide (LiTFSI)

 doi:10.20944/preprints201808.0145.v1

ABSTRACT

Considering the safety issues of Li ion batteries, all-solid-state polymer electrolyte has been one of the promising solutions. In this point, achieving a Li ion conductivity in the solid state electrolytes comparable to liquid electrolytes (>1 mS/cm) is particularly challenging. Employment of polyethylene oxide (PEO) solid electrolyte has not been not enough in this point due to high crystallinity. In this study, hybrid solid electrolyte (HSE) systems are designed with $Li_{1.3}Al_{0.3}Ti_{0.7}(PO_4)_3$(LATP), PEO and Lithium hexafluorophosphate ($LiPF_6$) or Lithium bis(trifluoromethanesulfonyl)imide (LiTFSI). Hybrid solid cathode (HSC) is also designed using LATP, PEO and lithium cobalt oxide ($LiCoO_2$, LCO) – lithium manganese oxide ($LiMn_2O_4$, LMO). The designed HSE system displays 3.0×10^{-4} S/cm (55 ℃) and 1.8×10^{-3} S/cm (23 ℃) with an electrochemical stability as of 6.0V without any separation layer introduction. Li metal (anode)/HSE/HSC cell in this study displays initial charge capacity as of 123.4/102.7 mAh/g (55 ℃) and 73/57 mAh/g (25 ℃). To these systems, Succinonitrile (SN) has been incorporated as a plasticizer for practical secondary Li ion battery system development to enhance ionic conductivity. The incorporated SN effectively increases the ionic conductivity without any leakage and short-circuits even under broken cell condition. The developed system also overcomes the typical disadvantages of internal resistance induced by Ti ion reduction. In this study, optimized ionic conductivity and low internal resistance inside the Li ion battery cell have been obtained, which suggests a new possibility in the secondary Li ion battery development.

Preprints (www.preprints.org) | NOT PEER-REVIEWED | Posted: 7 August 2018 doi:10.20944/preprints201808.0145.v1

Introduction

Li ion batteries have been credited for a great revolution of the strong intermittent renewable-energy sources replacing fossil fuels. They also critically contribute to the development of communication and transportation by the rise of super-slim smart phones and electric cars in a practical range. However, since announced in 1991, heels of Li ion battery phones and laptops have been recalled because of a flame causing injury to the users[1]. The cycle life is very limited because of poor cycling efficiency of Li electrode. The secondary cells are more sensitive to impurities such as water in the electrolyte and the electrode materials. And the cells under running would have Li dendrites leading to occasional explosions. Nonetheless, because of radical needs for high energy density and reliability of batteries, Li technology has been ceaselessly focused on. With high energy density and large capacity suitable for energy storage systems, Li ion is almost unique with low atomic weight compared to all other negative electrode materials that had been ever investigated.

The typical Li ion batteries consist of a negative anode, a positive cathode and a liquid electrolyte. However, many energy storage devices based on combustible organic solvents inevitably carry the risks of leakage, heavier packaging and related hazards. A liquid electrolyte is volatile at high temperature when the battery is charged or discharged quickly or when packs of car batteries are damaged in accidents. Against inherent disadvantages of liquid electrolytes[2–3], solid electrolytes of nonflammable polymers[4–5] and all-solid-state battery using inorganic materials[6-7] have been developed. When a battery releases power, lithium ions move from the anode through the electrolyte to the cathode. In this point, more conductive electrolyte generates better battery performance. Therefore, the promise of Li ion solid-state batteries is the replacement of the heavy and sometimes dangerous liquid electrolyte with a lighter, more versatile solid alternative. Although finding a solid electrolyte with conductivity comparable to liquids has been still a challenge, the solid electrolyte batteries are safer because flammable components are removed and deliver more power in which the carbon-based anodes can be replaced with lithium metal. This leads to a higher energy density and cycle life, with less weight and cost. In addition, without the need to struggle to safely pack a liquid electrolyte in a shape, all-solid-state batteries can be fabricated in more versatile shapes reducing manufacturing costs. This could make electric cars a more enticing proposition with longer running distance and a lower purchase price.

Preprints (www.preprints.org) | NOT PEER-REVIEWED | Posted: 7 August 2018 doi:10.20944/preprints201808.0145.v1

In many ways, all-solid-state constructions certainly enhance the overall performance of energy storage and conversion[8–10].

A potential solution against the disadvantage of solid-state electrolytes has been pursued[11–15]. In this point, the conductivity of polymer electrolytes such as polyethylene oxide (PEO) is explained in terms of the electron donating activity, weak coordinate bond and hopping of Li ions[16–17]. As a solid polymer electrolyte, alkali crystalline complexes of PEO with metals have been investigated because of significant ion conductivity[18–22]. However, Li agent in PEO has not been enough to generate effective ionic conductivity because high crystallinity of PEO bothers the Li ion movement[5]. Amorphous sites of PEO contribute to enhance the Li ion movement especially at room temperature[22–26]. When the PEO complex with relatively low glass transition temperature (T_g) becomes amorphous the ion conductivity exhibit 10^{-5}~10^{-4} cm^{-1} corresponding to 3~4 times higher than those of crystallites. However, when PEO complex displays liquid-like property which simultaneously induces short-circuits.

Oxide solid electrolytes. Inorganic oxides have been designed for electrolyte components[27–30], such as Perovskite-structured $Li_{3x}La_{2/3-x}TiO_3$[27], Garnet-structured $Li_7La_3Zr_2O_{12}$ (LLZO)[28–29], NASICON-structured $Li_{1+x}Al_xTi_{2-x}$ (LATP)[30]. Low conductivity (10^{-4}~10^{-3} S/cm), high grain boundary resistance and high calcination temperature of these oxide solid electrolytes cause increased volatility, phase transition and impurity, decreasing the total quality of Li ion battery. On the other hand, sulfide-based solid electrolyte including $Li_{10}GeP_2S_{12}$ (LGPS) display high conductivity almost similar to that of liquid electrolytes[31]. However, it is smelly, expensive, unstable under air and reactive with water generating harmful H_2S. A battery system composed of lithium aluminum germanium phosphate (LAGP, $Li_{1.5}Al_{0.5}Ge_{1.5}(PO_4)_3$,) and PEO has been tried with protecting layers[32]. The drawback of this system is a specific interaction of LAGP with Li metal and working at 50 °C but not at room temperature. One of the oxide solid electrolytes, lithium aluminum titanium phosphate (LATP) is highly stable under air and inexpensive. But LATP exhibits lower ion conductivity than that of liquid electrolyte or sulfide-based electrolytes, reduction of Ti^{4+} into Ti^{3+} by the interaction of Li ion, and high grain boundary resistance[33]. To overcome these problems, protecting layer of thin layers composed of PEO[34] or Al_2O_3[35] has been introduced to minimize the interaction with Li ion. LATP pellet was dip-coated in PEO for a protecting layer formation between the LATP and Li metal surface. However, due to low ionic conductivity of PEO itself, the whole system

Preprints (www.preprints.org) | NOT PEER-REVIEWED | Posted: 7 August 2018 doi:10.20944/preprints201808.0145.v1

exhibits 5.03×10^{-6} S/cm at 23 °C[36]. In this study, battery systems are designed without protecting layers, which effectively work at room temperature.

Succinonitrile (SN) Introduction. The lithium bis(trifluoromethanesulfonyl)imide (LiTFSI) exhibits limitation in narrow electrochemical windows (~4.8V) and low electrochemical stability[37–38]. To overcome these disadvantages, nonionic polymeric crystalline with excellent electrochemical stability is obtained by using succinonitrile (SN). Nitrile compounds are typically safe against fire and chemically stable at harsh conditions. SN has T_g of –40 °C and melting temperature (T_m) of 55 °C. Between these temperatures SN suppresses the crystallization of PEO and increases the physical stability against short-circuit. In addition, SN is highly polar to enhance the Li salt dissolution and movement. When SN forms a complex with LiTFSI, the conductivity increases up to 1×10^{-3} S/cm (25 °C) due to molecular rotation and trans-gauche isomerism[39–40]. Even though LGPS is relatively expensive and reactive with water generating unfavorable H_2S[41], LGPS+PEO+SN hybrid system does not bother Li ion movement thus conductivity due to SN contribution[42]. Using relatively inexpensive LAGP, LAGP+PEO and LAGP+PEO+SN hybrid systems have been developed[43]. The chemical reactivity of Li ions with solid electrolyte determines the ionic conductivity but this has not been fully investigated for LAGP+PEO+SN hybrid systems. In addition, the lattice structure of solid electrolytes modified by Ti ion reduction affects the Li ion movement. The complex composed of Ti^{4+} typically generates the conductivity close to 10^{-3} S/cm while that of Ti^{3+} significantly decreases the conductivity to 10^{-7} S/cm. The LAGP, PEO and SN system without protecting layer has been tried[35,43] but there is a lack of systematic electrochemical analysis to verify the interaction with Li ion.

In this study, all-solid-state Li ion batteries using designed hybrid solid electrolytes (HSEs) are investigated to overcome the disadvantages of PEO-only battery systems. Compromising the properties of LATP, SN are utilized for increased mechanical property and reduced possibility of short-circuits. In addition, disadvantageous grain boundary resistance of LATP is overcome by PEO introduction. Ion conductivity is prominently enhanced at room temperature by using effective dissolution of SN complex with LiTFSI and PEO. The chemical reaction is monitored by the day-by-day changes in impedance considering the physical interaction of LATP and Li metal. The reduction of Ti ion is investigated by using X-ray photoelectron spectroscopy (XPS) after the charging-discharging repetition. Linear

Preprints (www.preprints.org) | NOT PEER-REVIEWED | Posted: 7 August 2018 doi:10.20944/preprints201808.0145.v1

scanning voltammetry (LSV) curves of the designed electrodes confirm the extended region of electrochemical windows of PEO-only system which is originally narrow near 4.8V.

Results

Design of hybrid solid electrolytes (HSE) and hybrid solid cathode (HSC). This study introduces designed hybrid solid electrolyte (HSE) and hybrid solid cathode (HSC). The designed HSCs are combined with lithium ion manganese oxide (LMO, $LiMn_2O_4$ or Li_2MnO_3) and lithium cobalt oxide (LCO, $LiCoO_2$). In **Table 1**, composition and ion conductivity of the designed HSC and HSE are summarized at two temperature conditions (23 and 55 °C).

Li ion-conducting polyethylene oxide (PEO) is mixed with lithium aluminum titanium phosphates (LATP) synthesized in this study (Experimental Section). This sticky white HSE slurry is casted on Al or Li metal foil. For better casting process, the viscosity of the slurry is modified by controlling the content of LATP and PEO as well as molecular weight of PEO. The battery efficiency is compared with lithium(trifluoromethanesulfonyl)imide (LiTFSI) and lithium hexafluorophosphate ($LiPF_6$). In addition, the function of succinonitrile (SN) is evaluated in terms of the interaction with PEO and LiTFSI. Ion conductivity is compared with pure PEO electrolyte (HSE-1) and PEO/LATP (20/80) composite electrolyte with $LiPF_6$ (HSE-2). With LiTFSI, PEO/LATP (20/80) composite electrolyte without (HSE-3) and with (HSE-4) SN incorporation are compared. Two types of LMO/LCO (30/30) based cathodes are compared containing PEO/LATP (12.8/12.8) composite combined with LiTFSI, without (HSC-1) and with (HSC-2) SN incorporation

A representative coin cell preparation using the designed HSE-4 and HSC-2 is illustrated in **Fig. 1a**. The slurry is coated on anodic Li metal foil by solution casting. LATP, PEO, LiTFSI and SN are mixed in a designed composition using a centrifugal mixer (Thinky Mixer) resulting in a sticky white HSE-4 slurry. LMO and LCO are mixed with PEO and SN, resulting in HSC-2. The HSC-2 is coated on Al foil, followed by HSE-4 slurry casting. The Li metal anode and the designed cathode plates are bonded by heating HSE sides to form a layered structure of a coin cell. In addition, this process is scaled-up for a pouch cell (5 ×10 cm^2) in which copper foil is additionally employed outside of the Li metal plate for physical protection (**Fig. 1b**). The designed all-solid-state Li ion pouch battery is successfully working

Preprints (www.preprints.org) | NOT PEER-REVIEWED | Posted: 7 August 2018 doi:10.20944/preprints201808.0145.v1

even at the broken situation without any leakage and short-circuits (Supporting Information, Movie S1).

Structure of the all-solid-state battery system. The simplified battery sample is prepared to investigate the performance of HSE and HSC, which are casted and dried on a carbon tape in a layered structure stacked from Al foil, cathodic (HSC-2) and electrolyte (HSE-4) layers without anodic Li metal and protective Cu foil layers. A representative scanning electron microscopy (SEM) image of each layer is shown in a cross-sectional side-view (**Fig 2a**) and in a top-view (**Fig 2b**). In the cross-sectional image, the size of particulates in HSC layer (below the dotted-line in the picture) is smaller compared with those in the HSE layer, this is caused from relatively small size of the LCO and LMO particles (**Fig 2c**). The images of pure LATP powder at the same resolutions are compared in **Fig 2d**. The top-view images of the designed battery system (Fig 2b) are similar to those of the LATP powder pellet (Fig 2d). For all the systems, the inter-particulate spaces are effectively filled with PEO binding. The SEM images confirm effective physical contact of ion-conducting PEO and solid LATP in the designed HSE layer without phase separation, which is crucial for high ionic conductivity of a battery. Fig. 2b depicts the reticulated PEO connects LATP particles forming ion-conducting pathways, which can decrease boundary resistance in the solid LATP electrolyte. All of these morphologies are advantageous for the increase in the bulk ionic conductivity[44].

Conductivity of the designed systems. The total resistance is evaluated by ionic conductivity based on the electrochemical impedance spectroscopy (EIS) (Table 1). Using the measured resistance and following relation, ionic conductivity (σ, S/cm) of the designed HSE and HSC is evaluated,

$$\sigma = \frac{l}{A \cdot S} \quad (1)$$

where, l is the thickness (cm) of the HSE, A is the area (cm^2) of the sample, S is the total resistance (Ω) obtained from EIS spectra. The ionic conductivity of the designed HSE shows almost three orders higher (~10^{-4} S/cm) than that of pure PEO (10^{-6}~10^{-8} S/cm)[45] at the same EO to Li (8:1). This result confirms the contribution of high ionic conductivity of LATP embedded in the ion-conducting PEO by the reduced bulk and boundary resistance. Due to characteristic temperature-dependence[46], ionic conductivity at 55 ℃ is about 10 times higher than that at 23 ℃ in every sample. The composite system consists of LiTFSI shows similar ionic conductivity with those using $LiPF_6$. By adding SN, ionic conductivities (3×10^{-4} S/cm

Preprints (www.preprints.org) | NOT PEER-REVIEWED | Posted: 7 August 2018 doi:10.20944/preprints201808.0145.v1

@ 23 °C & 1.8×10^{-3} S/cm @ 55 °C) are enhanced compared with those (1.5×10^{-4} S/cm @ 23 °C & 1.4×10^{-3} S/cm @ 55 °C) without SN introduction by increased segmental mobility of PEO in HSE[47–48]. Especially the increase of ionic conductivity by SN introduction is prominent at room temperature than that at 55 °C.

Solid electrolyte interface (SEI). Even with several controversies[49–50] the LATP and Li metal is reported to react immediately upon a physical contact and forms unfavorable solid electrolyte interface (SEI) layer on the Li metal surface. This unfavorable phenomenon bothers the Li ion movement thus decreases the ionic conductivity. However, this is suppressed by surface modification using stealthy PEO coating[51]. The role of PEO in HSE is, at the same context, surrounding each LATP particle to protect the Li metal surface. The efficacy of the designed HSE on Li metal anode is investigated by measuring the AC impedance as a function of time (**Fig 3**). Impedance (Z) is composed of reactance and resistance by the relation,

$$Z = R + jX \tag{2}$$

where, the real part R is the resistance, while imaginary part X is the reactance. The chemical reaction of the designed model cells symmetrically composed of Li/LATP/Li and Li/HSE/Li are evaluated for 25 days. Among them, selected results of Li/LATP/Li (**Fig 3a**), Li/HSE-1/Li (**Fig 3b**) and Li/HSE-4/Li (**Fig 3c**) are shown. The increase in the resistance and reactance has been observed in the system of LATP/Li metal[51] and PEO/Li metal by the characteristic chemical reactions[37]. The interfacial resistance of the symmetric cells designed as Li/LATP/Li (Fig 3a) and Li/HSE-1/Li (Fig 3b) continuously increase the resistance and reactance for 25 days. However, the resistance of the Li/HSE-4/Li cell maintains almost similar low value for total 25 days (Fig 3c). The result suggests that the reaction of HSE-4 on Li metal is far more effective than that of LATP.

In order to evaluate the impedance result aforementioned, X-ray photoelectron spectroscopy (XPS) measurements of the HSE samples are performed before and after the reaction with Li metals **(Fig. 3d**). For this, Ti peaks of HSE-4 pasted on Li metal after the dynamic charging-discharging procedures (blue line) are compared with HSE-4 on Al foil, the physical substrate (red line) employed as a standard. Exposed to air, Ti is mostly present as TiO_2 (Ti appears as Ti^{4+}). Deconvolution results in eight different peaks[52] correspond to four chemical states.

Preprints (www.preprints.org) | NOT PEER-REVIEWED | Posted: 7 August 2018 doi:10.20944/preprints201808.0145.v1

Doublet peaks consist of Ti $2p_{1/2}$ and Ti $2p_{3/2}$: two strong Ti^{4+} peaks, i.e., $2p_{1/2}$ (Ti^{4+}, 464.6 eV) and $2p_{3/2}$ oxide (Ti^{4+}, 458.8 eV), two Ti^{3+} peaks (457 eV and 463.1 eV) and two Ti^{2+} peaks (455.3 eV and 461.7 eV), as well as two metallic Ti peaks (454.3 eV and 460.5 eV). Even with physical contact of LATP with Li metal, the binding energy of two samples in this study is same. The resulting XPS has no difference where the Ti $2p_{1/2}$ and Ti $2p_{3/2}$ remains at the same energy position, indicating there is no Ti reduction (from Ti^{4+} to Ti^{3+})[51]. Therefore, there is no lattice structure change induced by Ti rearrangement which otherwise affects the Li ion movement thus electrical conductivity eventually.

The mean thickness (d) of an organic coating on Ti nanocrystals, formed by the chemical grafting in HSE, is related with the intensity (I) of the Ti $2p_{3/2}$ signal originating from the substrate in XPS measurements,[53]

$$I \propto I_0 \sigma \rho e^{-(d/\lambda \sin\Theta)} \quad (3)$$

where, σ is the cross section, ρ is the density of the element, λ is the inelastic mean free path and Θ is the angle between the sample and the detector. The σ is specific for each orbital and depends on the photon energy (decreasing with increased photon energy). The λ is a measure of how far an electron can travel in a solid before losing energy[54], this is dependent on the photon energy. If normal emission and a flat surface is assumed the angle contribution of the intensity can be neglected. The XPS result shows the evolution of Ti 2p peak with decreased actual film depth after interaction with Li for 25 days. Both Ti $2p_{3/2}$ and Ti $2p_{1/2}$ intensities are increased for Ti films on Li metal in comparison to that of the intact HSE on Al foil. This type of signal augmentation might be ascribed to the partial blocking effect of intact HSE on the escape of photoelectrons from Ti to vacuum. Therefore, the designed battery is suggested to have advantages in terms of SEI formation after the charge-discharge procedure.

Electrochemical stability. To investigate the electrochemical stability of each electrolyte layer, linear sweep voltammetry (LSV) are measured from 1.5 to 6 V for both reduction and oxidation procedure (**Fig. 4)**. The oxidative stability is measured from the open current voltage (OCV) sweeping the voltage up, and the reduction is measured sweeping the voltage down from the OCV. In the Fig. 4 the voltage was swept from ~2.2 V up to 6V and then down again to 2.2V. Both electrolytes HSE-3 and HSE-4 clearly show an onset of oxidation around 4V and 3.4V, respectively. After going to 6V, the electrolyte will be partially or completely

Preprints (www.preprints.org) | NOT PEER-REVIEWED | Posted: 7 August 2018 doi:10.20944/preprints201808.0145.v1

decomposed. For the sweeping down from that stage, the reductive stability was measured in a separate experiment. The liquid electrolyte used as a standard contrast is oxidized at 4.8V noticed by the sudden increase in current (blue line). HSE (HSE-3) and HSE+SN (HSE-4) are also oxidized even if the absolute current intensity is relatively lower than that of liquid electrolyte. This electrochemical investigation of the designed cells indicates protective film formation on the cathode surface at the first cycle which works as a solid electrolyte interphase (SEI) in liquid electrolytes. On the other hand, during the reduction procedure of both HSE-3 and HSE-4, the current is very low without noticeable peak in all voltage regions in this study. Since reduction generates no specific current peak, the HSE which includes LATP, PEO, LiTFSI and SN is electrochemically stable from 2.5 V to 6 V.

Property of the designed electrolytes. Due to inherent high boundary resistance, LATP hardly generates high ionic conductivity. A value of ca. 3.4×10^{-3} S/cm at 293 K, is among the highest conductivities reported for LATP-based systems.[55–56] To overcome this disadvantage, PEO is employed in this study. The structure of the PEO-incorporated system prepared on Al foil is investigated using X-ray powder diffraction (XRD) in **Fig 5a**. The XRD patterns of LATP-incorporated systems are almost similar[34]. XRD patterns of HSE films exhibit lower intensity by the polymer incorporation without peak broadening. With the SN incorporation, XRD peak intensity becomes far lower, indicating the dilution of the whole system. Nonetheless the lattice structure is effectively maintained.

The ionic conductivity and thermal characteristics are modified according to the molecular weight of the PEO, which changes from 1×10^5, 3×10^5 to 6×10^5 in this study. The segmental mobility of PEO is investigated using differential scanning calorimetry (DSC) (**Fig 5b**). With the increase of PEO molecular weight, the peak temperature increases from 65.741°C (PEO M_w =1×10^5), 67.663 °C (PEO M_w =3×10^5) and 68.157 °C (PEO M_w =6×10^5). Meanwhile, the magnitude of the heat density decreases from 178.31 J/g, 172.41 J/g to 170.87 J/g. However, the designed HSE systems with LATP and SN do not generate characteristic peak at the given condition in **Fig. 5c**. This indicates that incorporation of LATP and SN effectively broadens the amorphous state to the wide temperature ranges, increasing the ionic conductivity at that condition. The DSC result of the system consisting of LiTFSI has been verified to become amorphous phase when the ratio of the [EO]/[Li] is higher than ten[57]. In this study the system consisted of LiTFSI with the ratio [EO]/[Li] = 8 exhibits amorphous phase with the help of

Preprints (www.preprints.org) | NOT PEER-REVIEWED | Posted: 7 August 2018 doi:10.20944/preprints201808.0145.v1

SN introduction. Based on this ionic conductivity result, the system with higher molecular weight PEO M_w =6×10^5 is selected to get enhanced mechanical property for the design of HSE, while lower molecular weight PEO M_w =3×10^5 is employed for better mixing efficacy to design cathode electrode.

Capacity and 1st Coulomb efficiency of the designed coin cells. The **Fig 6a** shows specific capacity-voltage curves of the first charge-discharge cycles of the selected model cell systems. The 1st cyclic profiles of LCO-LMO/HSE/Li metal system for each designed HSE-2, HSE-3 and HSE-4 and HSC-2/HSE-2/Li metal are compared at 55 ℃. The HSE-2 curve has more polarization loss compared to other curves. Further, the plateau region is quite broader for other three cases compared to the discharge curve of HSE-2 in terms of the slope nature. Although the difference is small in all the systems, the result of HSE-2 shows slight disadvantage compared to other three systems. Electrochemical Impedance Spectroscopy (EIS) results at 55 ℃ (**Fig. 6b**) and room temperature (**Fig. 6c**) are shown. $LiPF_6$ is generally used for liquid electrolytes, while $LiClO_4$ and LiTFSI are favorably employed for solid electrolyte systems. The ionic conductivity of the designed HSE is not so different (Table 1) but the resistance and charge-discharge efficacy in the designed Li ion cell are far different. $LiPF_6$ (HSE-2) and LiTFSI (HSE-3, HSE-4& HSC-2) are used with PEO in this study, by which physical properties of HSE-2 are far different from other three systems.

However, for both $LiPF_6$ (HSE-1 & HSE-2 for this study) and LiTFSI incorporated systems (HSE-3 & HSE-4 and HSC-1 & HSC-2 for this study), the resistance of the system in actual Li ion cell state becomes twice at 55 ℃ and four-times of that at room temperature. In Li ion cell state, the re-crystallization kinetics of PEO has been effectively slowed by the use of Li salts and bulky anions[58]. The moisture generated by the electrode cooling, decomposes $LiPF_6$ into PF_5, leading to the resistance increase by the interaction between PEO and SEI[59]. By this effect, in addition to overcharging, the constant voltage region becomes broader during the charging process while capacity decreases during the discharging procedure. When moisture-resistant LiTFSI or LiTFSI+SN are used, aforementioned phenomena are reduced and capacity can be increased. In the system composed of LiTFSI+SN (HSE-4), SN promotes the Li ion dissolution, thus capacity increases far higher than that of LiTFSI-only (HSE-3). The charging-discharging process occurring at room temperature also shows similar results in three systems while the HSE-2 composed of $LiPF_6$ exhibits dramatic difference. This result

Preprints (www.preprints.org) | NOT PEER-REVIEWED | Posted: 7 August 2018 doi:10.20944/preprints201808.0145.v1

indicates that the moisture formation after the cooling procedure turns the $LiPF_6$ into PF_6 gas and SEI in PEO, where SEI decreases the efficiency of the battery function significantly.

Fig. 7a displays 1st charge-discharge profiles of the LCO-LMO/electrolyte/Li metal systems of selected HSE-4 and HSC-2 (both are based on LiTFSI+SN composition) at room temperature. This indicates that SN addition boosts the battery function compared with the cells employing $LiPF_6$ (HSE-2) and LiTFSI-only (HSE-3) are not working effectively at room temperature regardless of PEO molecular weight. The cells without SN (HSE-3) in electrolyte display 72 mAh/g at charging while 52 mAh/g at discharging as observed in Fig 6. On the other hand, SN incorporation (HSE-4) improves the property as of 78 mAh/g at charging while 59.7mAh/g at discharging. The difference is clearer by the C-rate performance (**Fig. 7b**). The C-rate values of each region are on the graph: 0.05 C, 0.1 C, 0.2 C, 0.5 C, and 0.05 C. At the 1st charging procedure, the capacity of each cell is 111.4 mAh/g (HSE-2), 118.5 mAh/g (HSE-3), 118.9 mAh/g (HSE-4), and 123.4 mAh/g (HSC-2), while at the discharging procedure, 96.2 mAh/g, 97.6 mAh/g, 99.9 mAh/g, and 102.7 mAh/g, respectively. Their Coulombic efficiency (also Faraday Efficiency) is 86.4%, 82.3%, 84.0%, and 83.2%, respectively by the ratio of discharged capacity to charged capacity.

Discussion

In this study, to select proper Li ion source for the designed HSE, $LiPF_6$ and LiTFSI have been employed and measured the internal resistance on actual charging-recharging repetition. The solid electrolyte LATP shows ion conductivity as of 3×10^{-3} S/cm at the state of Ti^{4+} but it becomes far lower at the state of Ti^{3+} due to structural deformation, bothering Li ion movement. The solid electrolyte interaction with Li ion promotes the reduction of Ti^{4+} into Ti^{3+}. In this point, LATP is not a good choice to be used with Li at the state of lower than 1.8V[60]. In this study, hybrid solid electrolyte (HSE) composed of LATP, PEO and SN is designed without protection layer. We observed that there is no reduction of Ti^{4+} into Ti^{3} which is investigated by Electrochemical Impedance Spectroscopy (EIS). In this point, we suggest a new electrolyte system advantageously utilized in secondary Li ion battery. Even without any protecting layer the designed system shows no reduction of Ti. This is confirmed by XPS and high Li ion conductivity as of 2.6×10^{-4} S/cm at room temperature. The interaction with Li is investigated by electrochemical impedance spectroscopy (EIS) which verifies that the designed cell is working properly without protecting layer.

Preprints (www.preprints.org) | NOT PEER-REVIEWED | Posted: 7 August 2018 doi:10.20944/preprints201808.0145.v1

In addition to new hybrid solid electrolyte (HSE), new hybrid solid cathode (HSC) systems are designed and investigated, composed of LATP, PEO, LiTFSi (or $LiPF_6$) and SN. Typically employed for mass-production, slurry casting methods are utilized followed by lamination to reduce contact resistance. According to the type of Li salts (LiTFSi or $LiPF_6$), the designed HSE and HSC exhibit differentiated ion conductivity at two temperatures (25 and 55°C). In addition, during the dynamic charge-discharge procedure of the designed Li ion cells, the effect of internal resistance on the charge-discharge procedure and C-rate changes are investigated. In terms of the ion conductivity, the HSE with $LiPF_6$ and LiTFSI exhibit 1.2 and 1.5×10^{-4} S/cm, respectively. However, when these HSE is incorporated into the dynamic cell function, the internal resistance decreases four-times. This leads to a greatly improved capacity by the difference of 1st charge-discharge and over-charge of each cell, which is more prominent at room temperature than at 55 °C.

Conclusion

The moisture induced by the cooling procedure inevitably decomposes $LiPF_6$ into PF_5 gas and SEI which reacts with PEO. With this phenomenon internal resistance increases thus LiTFSI is preferred over $LiPF_6$ for PEO-based Li ion battery cell. In this study the advantageous usefulness of LiTFSI is verified in this respect. The interaction of LATP with Li ions is investigated with the designed HSEs. XRD results after the charge-discharge procedure confirms that there is no Ti reduction ($Ti^{4+} \rightarrow Ti^{3+}$) which can modify the lattice structure thus the ion conductivity. LATP and Li ions are not reacted for 25 days without any increase in resistance. LATP has been reported to actively reactive with Li ions. This study sheds new light on the usefulness of LATP. With the help of the SN, the amorphous state of PEO becomes more stable contributing to increased ion conductivity.

LiTFSI and SN delay the crystallization of PEO, expanding the range of amorphous state thus leading to increase in ion conductivity. This study contributes to design and manufacturing of moderate-price Li ion batteries and their mass–productions. The grain boundary resistance, a typical disadvantage of oxide solid electrolyte has been decreased by using designed HSE in this study as well as solution casting process and lamination. We have successfully overcome typical disadvantages of solid electrolytes and developed all-solid-state secondary Li ion battery which is stable and effective for commercial use. This study contributes to a new design technology and further possible mass-production of Li ion battery in more economical and effective ways.

Preprints (www.preprints.org) | NOT PEER-REVIEWED | Posted: 7 August 2018 doi:10.20944/preprints201808.0145.v1

Experimental Section

Chemicals. All chemicals were purchased and used without further purification: Conductive carbon black (Super-P, Timcal ,Canada), Li_2O_3 (Lithium carbonate, 99%, Sigma-Aldrich, USA), Al_2O_3 (Aluminum oxide, 99.99%, Sigma-Aldrich, USA),TiO_2 (Cotiox KA-100, 98%, Cosmo Chemical, South Korea),$NH_4H_2PO_4$ (Ammonium dihydrogenphosphate, 99.999%,Sigma-Aldrich, USA), PEO (Poly(ethylene oxide, M_W =1×10^5, 3×10^5 and 6×10^5, Sigma-Aldrich, USA),LiTFSI (Bis(trifluoromethane) Sulfonimide lithium salt, 99.95%, Sigma-Aldrich, USA), $LiPF_6$ (Lithium hexafluorophosphate, 99.99%, Sigma-Aldrich, USA), AN (Acetonitrile Anhydrous, 99.8%, Sigma-Aldrich, USA), SN (Succinonitrile, 99%, Sigma-Aldrich USA), LCO (PoscoESM, South Korea), LMO (G05, ILJIN materials, South Korea).

Synthesis of LATP. The solid electrolyte LATP ($Li_{1.3}Al_{0.3}Ti_{0.7}(PO_4)_3$) was synthesized by a conventional solid-state method. Stoichiometric amount of Li_2CO_3, Al_2O_3, TiO_2, and $(NH_4)H_2PO_4$ were mixed in a ball mill for 12 hr. The slurry was sintered in a furnace at 900 ℃ for 2 hr. The dried powder was then jet milled at 1800 rpm for 2 hr to reduce the particle size. D-values (D_{10}, D_{50} & D_{90}) are measured for particle size evaluation as an intercept for 10%, 50% and 90% of the cumulative mass and D_{50} ~ 6 μm is obtained for effective mixing process.

Preparation of hybrid solid electrolytes (HSE) and hybrid solid electrolyte cathode (HSC). Li ion conducting polymer PEO is mixed with LiTFSI ([EO]:[Li]=8:1) and previously synthesized LATP (LATP:PEO=8:2 by weight) in acetonitrile (AN). The polymer solution is mixed using centrifugal mixer (THINKY mixer ARM-310) by 2000 rpm for 15 min. Then, with or without 5 wt. % of SN (Succinonitrile). The slurry is mixed again for 15 min. For the tests, this HSE slurry is casted on Al foil for analysis or on an electrode for coin cell test. After natural drying at room temperature for 1 hr, they are dried completely at 50 ℃ vacuum oven for 12 hr.

For better binding in the electrode, higher molecular weight of PEO (M_w~ 3×10^5 and 6×10^5) were employed. LATP, PEO (LATP:PEO=5:5 by weight) and LiTFSI ([EO]:[Li]=10:1) were mixed in AN using THINKY mixer for 15 min. $LiMn_2O_4$ and $LiCoO_2$ as active materials and Super-P as conductive material were added in additional solvent AN, followed by mixing for 15 min. After the HSC slurry was casted on Al foil by doctor blade, the electrodes were dried at 80 ℃ vacuum oven for 24 hr. HSE slurry was casted on the dried electrode and Li metal. The HSC/HSE composite was dried at the aforementioned condition. Differing from cathode

Preprints (www.preprints.org) | NOT PEER-REVIEWED | Posted: 7 August 2018 doi:10.20944/preprints201808.0145.v1

side, Li metal/HSE composite was dried at room temperature for 24 hr to avoid crumble. To evaluate the electrochemical performance, the CR2032 coin-type cell was fabricated with HSC/HSE composite and Li metal/HSE by laminate process. The construction of the cell is described as Fig. 1. All process was conducted in dry-room.

Characterization. Synthesized LATP and the HSC/HSE composites were observed using scanning electron microscope (SEM, SEC MiniSEM SNE-3000M) and X-ray diffraction (XRD, Rigaku MiniFlex600). XRD patterns of samples were obtained over a 2θ range from 10 deg to 80 deg with Cu Kα radiation at room temperature. The scan rate was 6 deg/min. Linear sweep voltammetry (LSV) was performed for both oxidation and reduction procedure for selected samples using potentiostat (Bio Logic SP-150) with scan rate of 20 mV/s from OCV to 1.5 V or 6.0 V. Ionic conductivity is calculated by AC impedance method with symmetric SS/Al/HSE/Al/SS cell using multi-channel potentiostat (Bio Logic VMP3). The samples were placed at 25 ℃ and 55 ℃ for 10 min, then analyzed from 500 kHz to 1 Hz at open-circuit voltage with 5.0 mV amplitude. With differential scanning calorimeter (DSC, DISCOVERY DSC2500), the calorimetric measurement is performed from room temperature to 100 ℃ at the heating rate of 10℃/min. The cell is cycled from 3 V to 4.3 V with 0.05 C for formation or each C-rate (1C = 1.5 $mAcm^{-1}$) at room temperature or 55℃.

Acknowledgments

This research was supported by the Industrial Fundamental Technology Development Program (10052745, Development of the nano-sized (100 nm) manganese ceramic material for high voltage pseudo-capacitor) funded by the Ministry of Trade, Industry and Energy (MOTIE) of Korea.

Author Contributions

S. Cho carried out synthesis and characterization, prepared data and supporting information and Figures; S. Cho, S. Kim, W. Kim, S. Kim, S. Ahn contributed to discussions and text preparation; S. Ahn wrote the manuscript and contributed to discussions, text preparation. S. Cho and S. Ahn generated the concept of the study. All the authors contributed to revised and completed the manuscript.

 doi:10.20944/preprints201808.0145.v1

Additional Information

Supplementary information accompanies this paper https://www.nature.com.

Competing Interests: The authors declare no competing interests.

Publisher's note: Springer Nature remains neutral with regard to jurisdictional claims in published maps and institutional affiliations.

Preprints (www.preprints.org) | NOT PEER-REVIEWED | Posted: 7 August 2018 doi:10.20944/preprints201808.0145.v1

Captions

Table 1. Composition of the designed hybrid solid electrolyte (HSE) and hybrid solid cathode (HSC) in this study. The ionic conductivities of HSE at 25 and 55 ℃ are shown. *PEO Mw =6×10^5 g·mol^{-1}, is used for HSE 1 to HSE 3, while PEO Mw = 3×10^5 g·mol^{-1} for HSC-1 and HSC-2. For the whole battery design, HSE-1 to HSE-3 are combined with HSC-1, but HSC-2 is only combined with HSE-4.

Figure 1. **(a)** Preparation of all-solid-state coin-cell using the designed HSE and HSC in this study. **(b)** Configuration of all-solid-state pouch cell in 5×10 cm^2 scale (left scheme) and its operation (right picture)

Figure 2. SEM images of **(a)** cross-section and **(b)** Top view of HSE-3/CHSE-1/Al foil on carbon tape **(c)** LCO and LMO and **(d)** LATP powder used in this study

Figure 3. Impedance spectra of **(a)** Li/LATP/Li **(b)** Li/HSE-1/Li **(c)** Li/HSE-4/Li symmetric cells as a function of time **(d)** Ti2p$_{3/2}$ and Ti2p$_{1/2}$ photoelectron signals of Ti films (HSE-4) coated on Li metal and Al foil.

Figure 4. Linear sweep voltammetry (LSV) scans of electrolyte with HSE-3 and HSE-4. Pt as a working electrode and Li metal is employed as counter and reference electrodes. Scan rate is at the 1 mV/s.

Figure 5. **(a)** XRD Patterns of LATP, HSE-3, HSE-4 **(b)** DSC of PEO with different molecular weight 1×10^5, 3×10^5 and 6×10^5 **(c)** DSC of HSE-3 (PEO 3×10^5), HSE-3 (PEO 6×10^5) and HSE-4 (PEO 3×10^5).

Figure 6. **(a)** 1st charge-discharge profiles of HSE-2, HSE-3, HSE-4 and HSC-2 at 55 °C. EIS profiles of **(b)** HSE-2 and HSE-4 at 55 °C and **(c)** HSE-2, HSE-3, HSE-4 and HSC-2 at room temperature.

Figure 7. **(a)** 1st charge-discharge profiles of LCO-LMO/electrolyte/Li metal with HSE-4 and HSC-2 at room temperature. **(b)** C-rate performance of LCO-LMO/electrolyte/Li cells with HSE-2, HSE-3, HSE-4, HSC-2 at 55 °C.

 doi:10.20944/preprints201808.0145.v1

REFERENCES

1. Julien, C., Mauger, A., Vijh, A., & Zaghib, K. *Lithium Batteries: Science and Technology,* p. 5, (Springer, New York, 2015).
2. Wang, Q. et al. Thermal runaway caused fire and explosion of lithium ion battery. *J. Power Sources* **208**, 210–224 (2012).
3. Santhanagopalan, S. et al. Analysis of internal short-circuit in a lithium ion cell. *J. Power Sources* **194**, 550–557 (2009).
4. Armand, M. & Tarascon, J. M. Building better batteries. *Nature* **451**, 652–657 (2008).
5. Wakihara, M., Kadoma, Y., Kumagai, N., Mita, H., Araki, R., Ozawa, K., Ozawa, Y. *Journal of Solid State Electrochemistry*. **16**, 847–855 (2012).
6. Goodenough, J. B. Ceramic solid electrolytes. *Solid State Ionics* 94, 17–25(1997).
7. Knauth, P. Inorganic solid Li ion conductors: an overview. *Solid State Ionics* **180**, 911–916 (2009).
8. Xu, K. Nanoqueous Liquid Electrolytes for Lithium-Based Rechargeable Batteries. *Chem. Rev.,* **104**, 4303–4418 (2004)
9. Goodenough, J. B. & Kim, Y. Challenges for rechargeable batteries. *J. Power Sources* **196**, 6688–6694 (2011)
10. Fergus, J. W. Ceramic and polymeric solid electrolytes for lithium-ion batteries. *J. Power Sources* **195**, 4554–4569 (2010)
11. Li, J., Ma, C., Chi, M., Liang, C. & Dudney, N. J. Solid electrolyte: the key for high-voltage lithium batteries. *Adv. Energy Mater.* **5**, 1401408 (2015).
12. Bachman, J. C. et al. Inorganic solid-state electrolytes for lithium batteries:mechanisms and properties governing ion conduction. *Chem. Rev.* **116**,140–162 (2015).
13. Xiayin, Y. et al. All-solid-state lithium batteries with inorganic solid electrolytes:review of fundamental science. *Chin. Phys. B* **25**, 018802 (2016).
14. Goodenough, J. B. & Singh, P. Review—solid electrolytes in rechargeable electrochemical cells. *J. Electrochem. Soc*. **162**, A2387–A2392 (2015).
15. Janek, J. & Zeier, W. G. A solid future for battery development. *Nat. Energy* **1**, 16141 (2016).
16. MacCallum, J. et al. *Polymer Electrolyte Reviews-1*. (Elsevier Applied Science, London and New York, 1987)
17. Nazri, A. et al. *Lithium Batteries Science and Technology. Kluwer* (Academic Publishers, New York, 2009)
18. Bailey, F. E. Jr., & Koleske, J. V. *Poly(ethylene oxide)* (Academic Press, New York, 1976)
19. Wright, P. V. Electrical conductivity in ionic complexes of poly(ethylene oxide). *Polymer International* **7**, 319–327 (1975)
20. Fenton, D. E. et al. Complexes of alkali metal ions with poly(ethylene oxide). *Polymer* **14**, 589 (1973)
21. Armand M. B.& Duclot M. Eur. Patent, 0013109, Prior. Fr. 7832976 (1978)
22. Armmd, M. B. *Polymer solid electrolytes – an overview. S. S. Ionics* 9-10, 745–754 (1983)
23. Ryu, S. W. et al. Effect of counter ion placement on conductivity in single-ion conducting block copolymer electrolytes. *J. Electrochem. Soc.* **152**, A158–A163 (2005)
24. Kang. W. et al. Synthesis and electrochemical properties of lithium methacrylate-based self doped gel polymer electrolytes. *Electro. Acta* **54**, 4540–4544 (2009)
25. Bruce, P. G. & Vincent, C. A. Steady state current flow in solid binary electrolyte cells. *J. E. C. I. Electrochem.* **225**, 1–17 (1987)
26. Kroka, F. et al. Impedance and polarization studies of new lithium polyelectrolyte gels. *J. Power Sources* **81**, 766–771(1999)
27. Stramare, S. et al. Structure and conductivity of B-site substituted (Li,La)TiO_3. *Mater. Sci. Engineering: B* **113**, 85–90 (2004)
28. Murugan, R. et al. Fast Lithium Ion Conduction in Garnet-Type $Li_7La_3Zr_2O_{12}$. *Angewandte Chem.* **46**, 7778–7781 (2007)
29. Hanc, E. et al. Fast Lithium Ion Conduction in Garnet-Type $Li_7La_3Zr_2O_{12}$. *Solid State Ion.* **262**, 617–621 (2014)

30. Aono, H. et al. Ionic Conductivity of Solid Electrolytes Based on Lithium Titanium Phosphate. *J. Electrochem. Soc*. **137**, 1023–1027 (1990)
31. Kato, Y. et al. Discharge Performance of All-Solid-State Battery Using a Lithium Superionic Conductor $Li_{10}GeP_2S_{12}$. *Electrochemistry* **10**, 749–751 (2012)
32. Wang, C., Yang, Y., Liu, X., Zhong, H., Xu, H., Xu, Z., Shao, H., & Ding, F. Suppression of Lithium Dendrite Formation by Using LAGP-PEO (LiTFSI) Composite Solid Electrolyte and Lithium Metal Anode Modified by PEO (LiTFSI) in All-Solid-State Lithium Batteries. *ACS Appl. Mater. Interfaces,* **9**, 13694–13702 (2017).
33. Han, X. et al. Negating interfacial impedance in garnet-based solid-state Li metal batteries. *Nat. Mater.* **16**, 572–579 (2017)
34. Wang, C. et al. Suppression of Lithium Dendrite Formation by Using LAGP-PEO (LiTFSI) Composite Solid Electrolyte and Lithium Metal Anode Modified by PEO (LiTFSI) in All-Solid-State Lithium Batteries. *ACS Appl. Mater. Interfaces* **9**, 13694–13702 (2017)
35. Jung, Y.-C. Lee, S.-M. Choi, J.-H. Jang, S. S. & Kim, D.-W. All Solid-State Lithium Batteries Assembled with Hybrid Solid Electrolytes. *J. Electrochem. Soc*. **162**, A704–A710 (2015).
36. Liu, W., Milcarek, R. J., Falkenstein-Smith, R. L. & Ahn, J. Interfacial Impedance Studies of Multilayer Structured Electrolyte Fabricated With Solvent-Casted PEO_{10}–$LiN(CF_3SO_2)_2$ and Ceramic $Li_{1.3}Al_{0.3}Ti_{1.7}(PO_4)_3$ and Its Application in All-Solid-State Lithium Ion Batteries. *J. Electrochem. En. Conv. Stor.* **13**, 021008 (2016).
37. Zhao, C. et al. A new solid polymer electrolyte incorporating $Li_{10}GeP_2S_{12}$ into a polyethylene oxide matrix forall-solid-state lithium batteries. *J. Power Sources* **301**, 47–53 (2016)
38. Chen, B. et al. A new composite solid electrolyte PEO/$Li_{10}GeP_2S_{12}$/SN for all-solid-state lithium battery. *Electro. Acta* **210**, 905–914 (2016)
39. Long, S. et al. Fast ion conduction in molecular plastic crystals. *Solid State Ion.* **161**, 105–112 (2003)
40. Alarco, P. J. et al. Highly conductive, organic plastic crystals based on pyrazolium imides. *Solid State Ion.* **175**, 717–720 (2004)
41. Ohtomo, T., Hayashi, A., Tatsumisago, M. & Kawamoto, K. Suppression of H2S gas generation from the 75Li(2)S center dot 25P(2)S(5) glass electrolyte by additives. *J. Mater. Sci.*, 48, 4137–4142 (2013).
42. Zhao, Y., Wu, C., Peng, G., Chen, X., Yao, X., Bai, Y., Wu, F., Chen, S., Xu, X. A new solid polymer electrolyte incorporating $Li_{10}GeP_2S_{12}$ into a polyethylene oxide matrix for all-solid-state lithium batteries. *Journal of Power Sources* 301, 47–53 (2016).
43. Jung, Y.-C., Park, M.-S., Doh, C.-H., Kim, D.-W. Organic-inorganic hybrid solid electrolytes for solid-state lithium cells operating at room temperature. *Electrochimica Acta.* **218**, 271–277 (2016).
44. Tatsumisago, M., Nagao, M., Hayashi, A. Recent development of sulfide solid electrolytes and interfacial modification for all-solid-state rechargeable lithium batteries. *Journal of Asian Ceramic Societies* 1 (1), 17–25 (2013).
45. Kim, J. G., Son, B., Mukherjee, S., Schuppert, N., Bates, A., Kwon, O., Choi, M.J., Chung, H.Y., Park, S. A review of lithium and non-lithium based solid state batteries, *J. Power Sources* **282**, 299–322 (2015).
46. Golodnitsky, D., Strauss, E., Peled, E. & Greenbaum, S. Review—On Order and Disorder in Polymer Electrolytes. *J. Electrochem. Soc.* **162**, A2551–A2566 (2015).
47. Jung, Y. C. et al. All Solid-State Lithium Batteries Assembled with Hybrid Solid Electrolytes. *J. Electrochem. Soc.* **162**, A704–A710 (2015)
48. Kim, S. K. et al. Lithium-Ion Cells Assembled with Flexible Hybrid Membrane Containing Li^+-Conducting Lithium Aluminum Germanium Phosphate. *J. Electrochem. Soc.* **163**, A974–A980 (2016)
49. Camacho-Forero, L. E., Smith, S. Bertolini, T. W. & Balbuena, P. B. Reactivity at the Lithium–Metal Anode Surface of Lithium–Sulfur Batteries. *J. Phys. Chem. C,* **119**, 26828–26839 (2015).
50. Lin, D., Liu, Y.& Cui, Y. Reviving the lithium metal anode for high-energy batteries. *Nat. Nanotechnol.* **12**, 194–206 (2017).
51. Hartmann, P. et al. Degradation of NASICON-Type Materials in Contact with Lithium Metal:

 doi:10.20944/preprints201808.0145.v1

Formation of Mixed Conducting Interphases (MCI) on Solid Electrolytes. *J. Phys. Chem. C* **117**, 21064–21074 (2013)

52. Fu, Y., Du, H., Zhang, S., Huang, W. XPS characterization of surface and interfacial structure ofsputtered TiNi films on Si substrate. *Mater. Sci. Eng. A* **403**, 25–31(2005).
53. Marinado, T. et al., *J. Phys. Chem. C* **114**, 11903 (2010).
54. Campbell J. L. & Rapp, T. Widths of the atomic K - N7 levels. *Atomic Data and Nuclear Data Tables* **77**, 1–56 (2001).
55. Aono, H., Sugimoto, E., Sadaoka, Y., Imanaka, N. & Adachi, G. Ionic Conductivity of Solid Electrolytes Based on Lithium Titanium Phosphate. *J. Electrochem. Soc.,* **137**, 1023–1027 (1990).
56. Takahashi, K., Ohmura, J., Im, D., Lee, D. J., Zhang, T., Imanishi, N., Hirano, A., Phillipps, M. B., Takeda, Y. & Yamamoto, O. A Super High Lithium Ion Conducting Solid Electrolyte of Grain Boundary Modified Li1.4Ti1.6 Al0.4(PO4)3. *J. Electrochem. Soc.*, **159**, A342–A348 (2012).
57. Geiculescu, O. E. et al. Transport Properties of Solid Polymer Electrolytes Prepared from Oligomeric Fluorosulfonimide Lithium Salts Dissolved in High Molecular Weight Poly(ethylene oxide). *J. Phys. Chem. B.* **110**, 23130–23135 (2006)
58. Vallee, A. et al. Comparative study of poly(ethylene oxide) electrolytes made with $LiN(CF_3SO_2)_2$, $LiCF_3SO_3$ and $LiClO_4$: Thermal properties and conductivity behavior. *Electro. Acta* **37**, 1579–1583 (1992)
59. Sloop, S. E. et al. The role of Li-ion battery electrolyte reactivity in performance decline and self-discharge. *J. Power Sources* **119**, 330–337 (2003)
60. Tanaka, K. et al. Lithium ion conduction in $LiTi_2(PO_4)3$. *Solid State Ionics* **139**, 241–247 (2001).

Preprints (www.preprints.org) | NOT PEER-REVIEWED | Posted: 7 August 2018 doi:10.20944/preprints201808.0145.v1

Table 1

		LATP (g)	PEO* (g)	$LiPF_6$	LiTFSI	SN (g)	LMO+LCO (g)	EO:Li (Mole ratio)	Ion. Con. @23℃ [S/cm]	Ion. Con. @55℃ [S/cm]
HSE	HSE-1	-	100	●	-	-	-	8:1	1.7×10^{-7}	1.0×10^{-6}
	HSE-2	80	20	●	-	-	-	8:1	1.2×10^{-4}	2.4×10^{-3}
	HSE-3	80	20	-	●	-	-	8:1	1.5×10^{-4}	1.4×10^{-3}
	HSE-4	80	20	-	●	5	-	8:1	3.0×10^{-4}	1.8×10^{-3}
HSC	HSC-1	12.8	12.8	-	●	-	30 + 30	10:1	-	-
	HSC-2	12.8	12.8	-	●	5	30 + 30	10:1	-	-

Preprints (www.preprints.org) | NOT PEER-REVIEWED | Posted: 7 August 2018 doi:10.20944/preprints201808.0145.v1

Figure 1

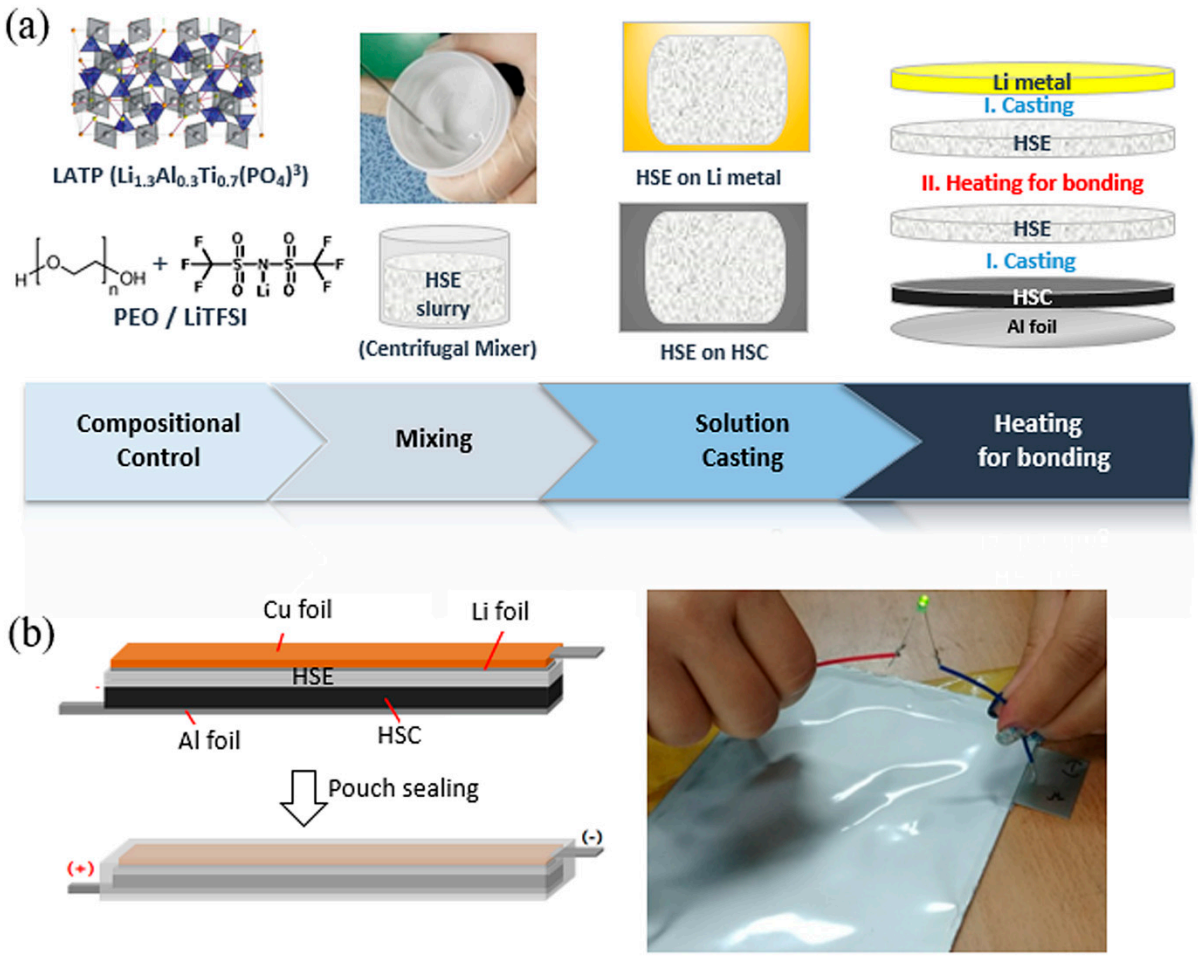

Preprints (www.preprints.org) | NOT PEER-REVIEWED | Posted: 7 August 2018 doi:10.20944/preprints201808.0145.v1

Figure 2

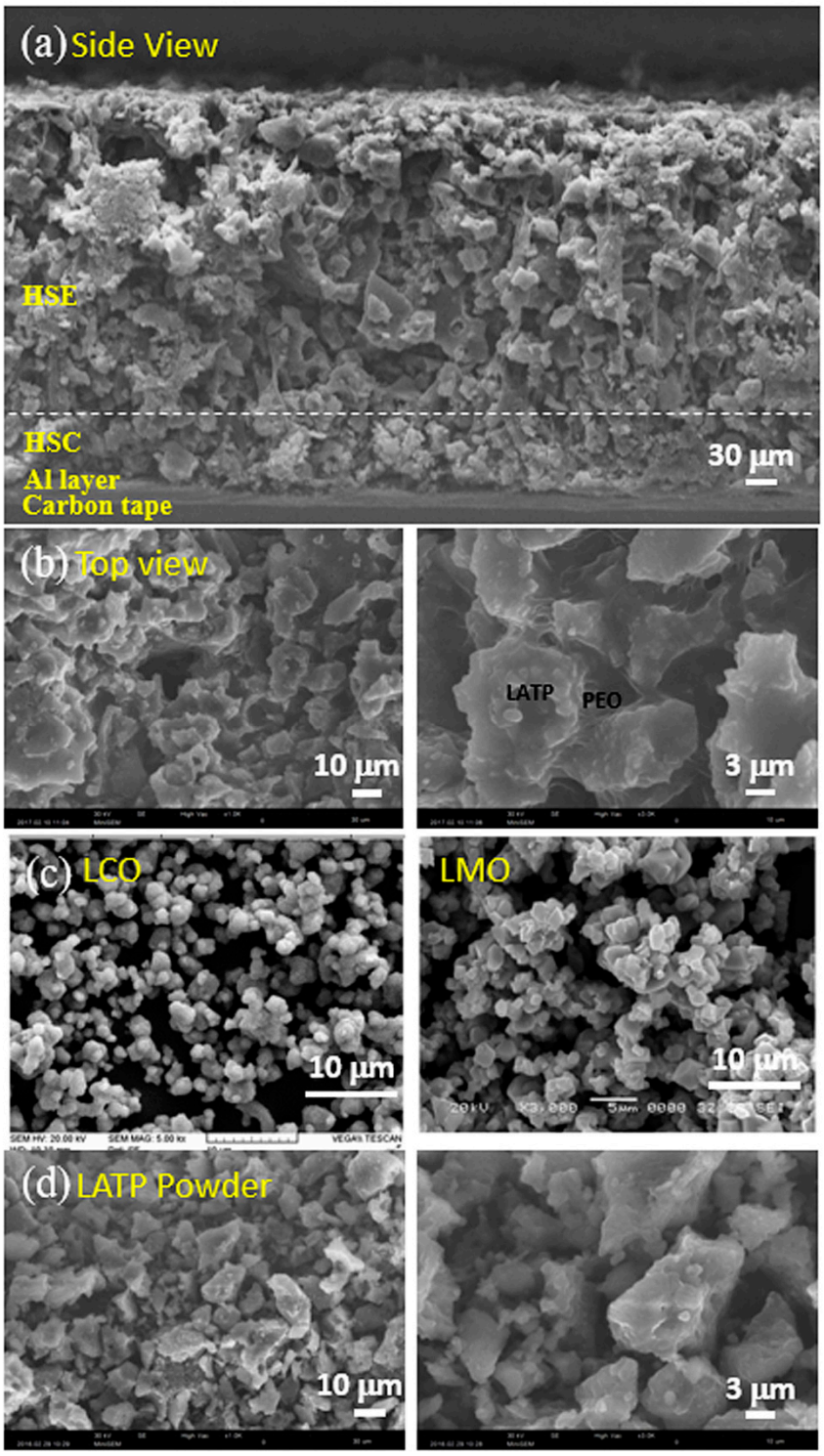

Preprints (www.preprints.org) | NOT PEER-REVIEWED | Posted: 7 August 2018 doi:10.20944/preprints201808.0145.v1

Figure 3

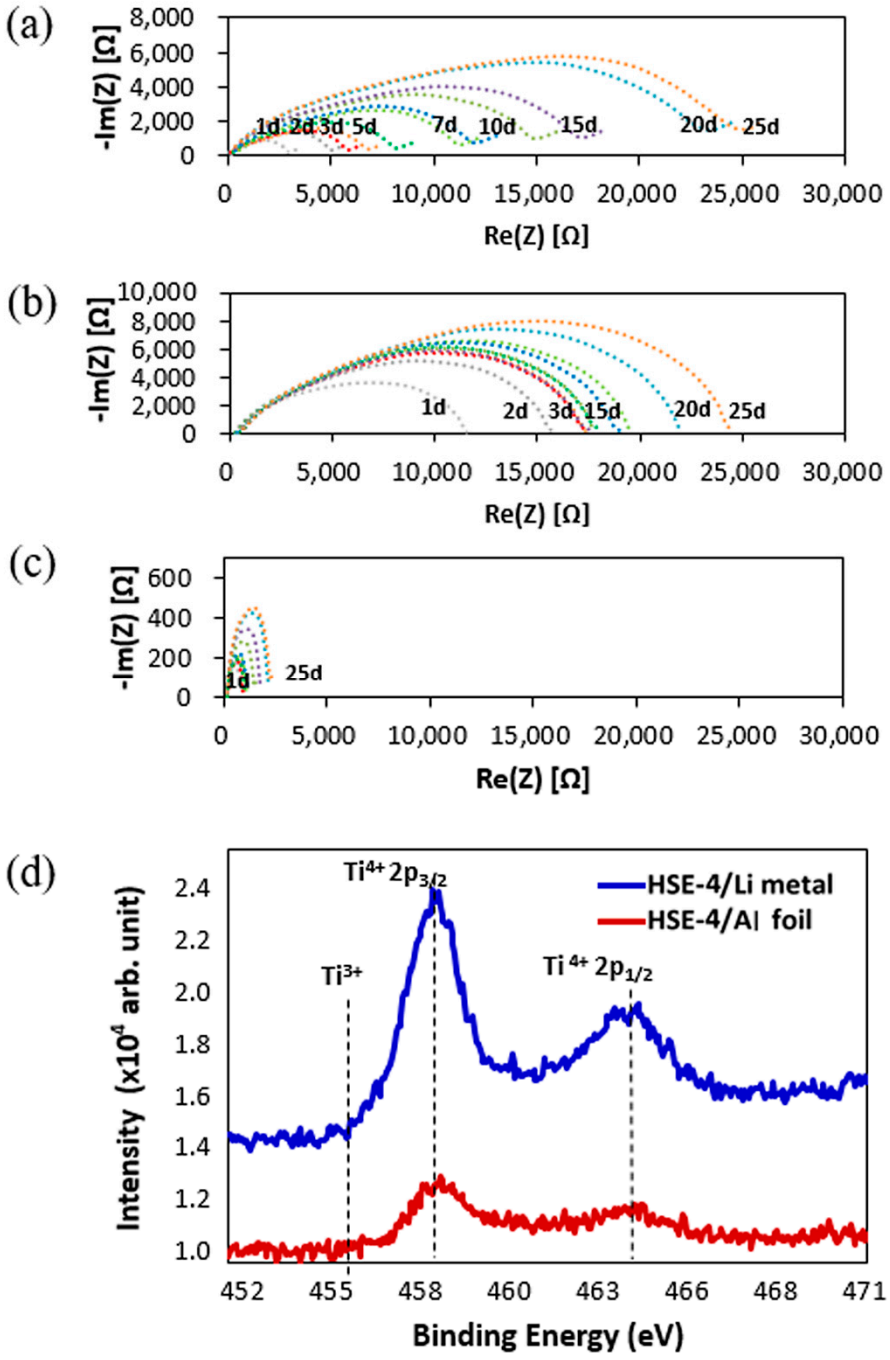

Preprints (www.preprints.org) | NOT PEER-REVIEWED | Posted: 7 August 2018 doi:10.20944/preprints201808.0145.v1

Figure 4

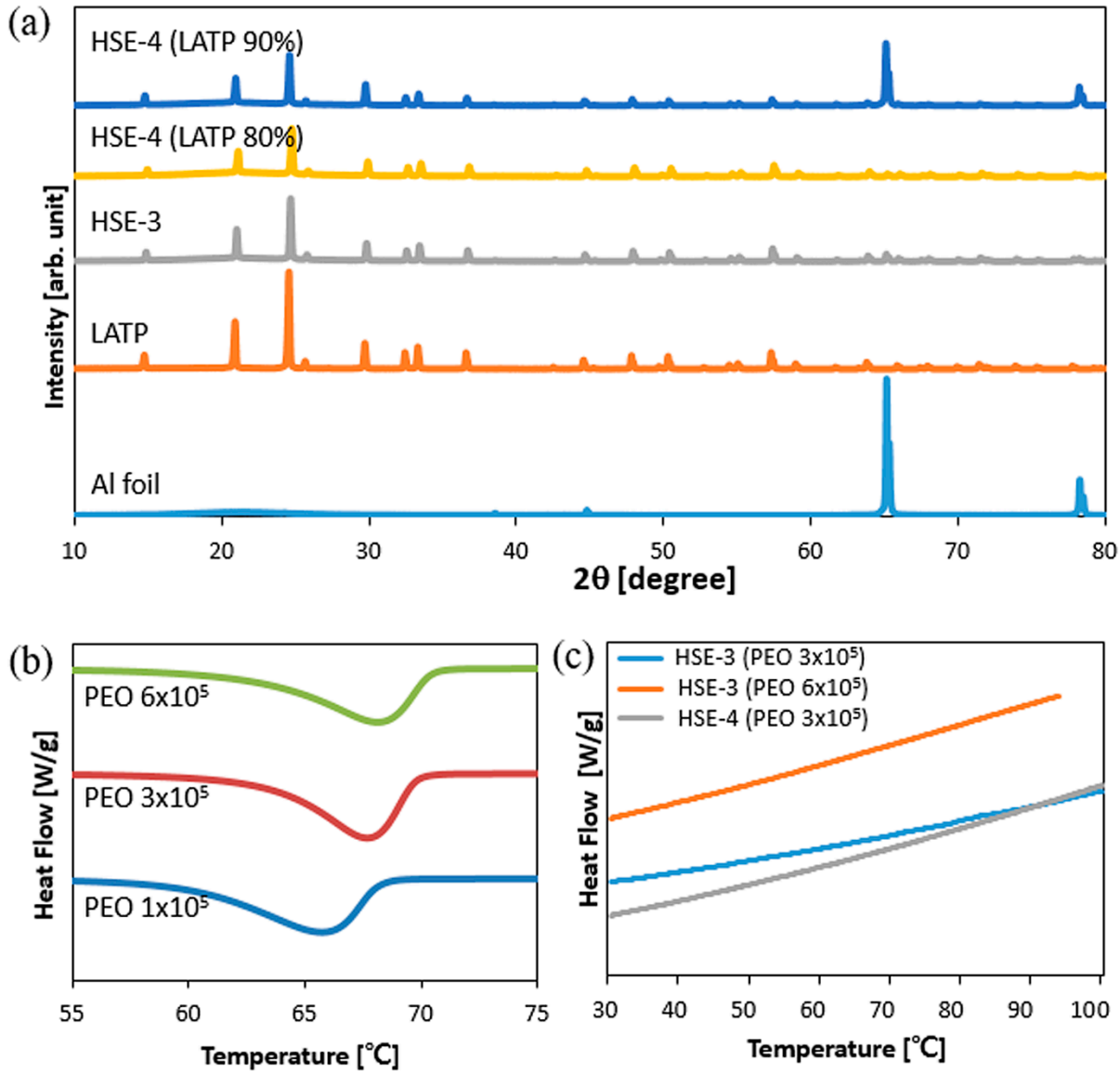

Preprints (www.preprints.org) | NOT PEER-REVIEWED | Posted: 7 August 2018 doi:10.20944/preprints201808.0145.v1

Figure 5

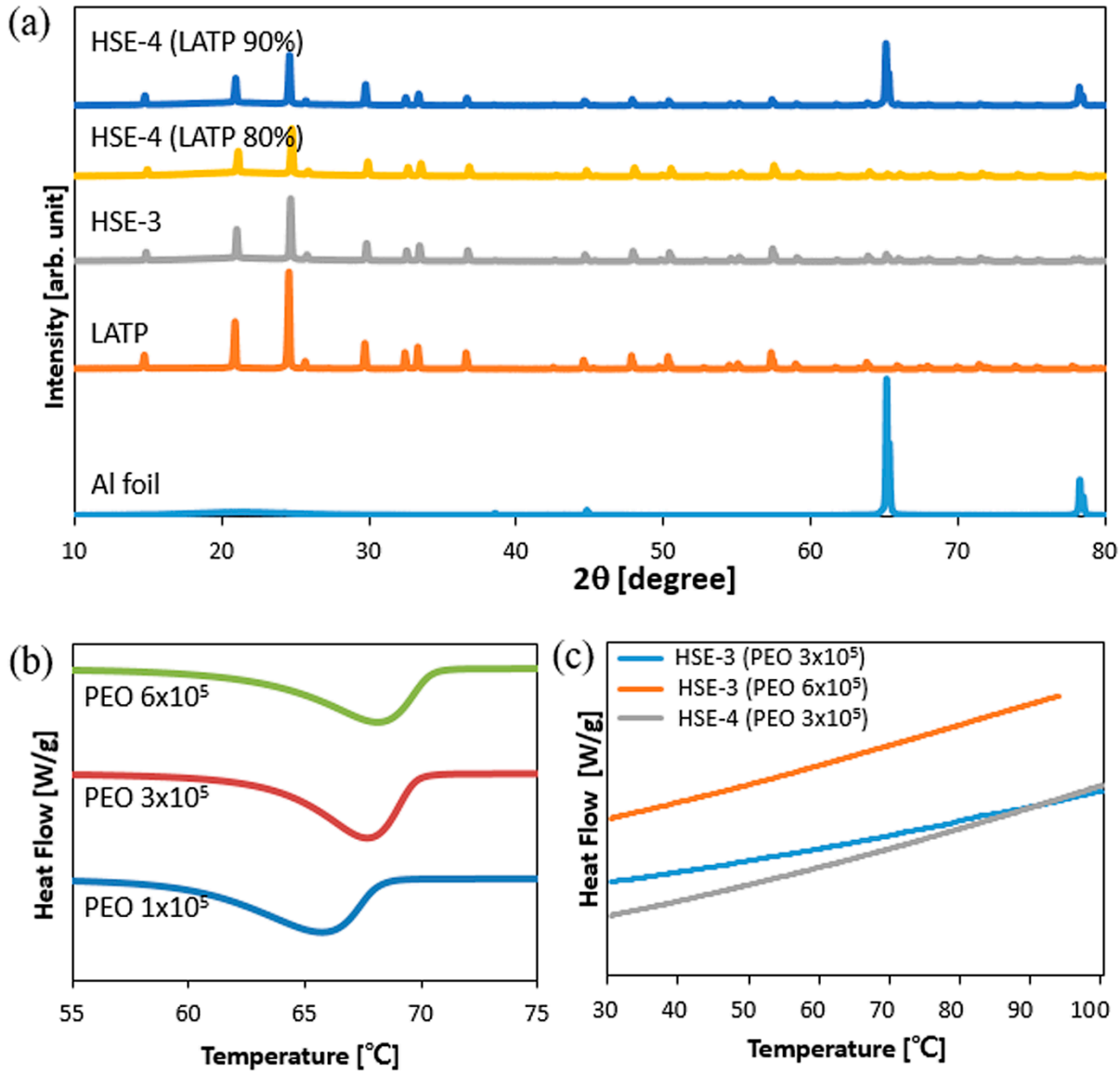

Preprints (www.preprints.org) | NOT PEER-REVIEWED | Posted: 7 August 2018 doi:10.20944/preprints201808.0145.v1

Figure 6

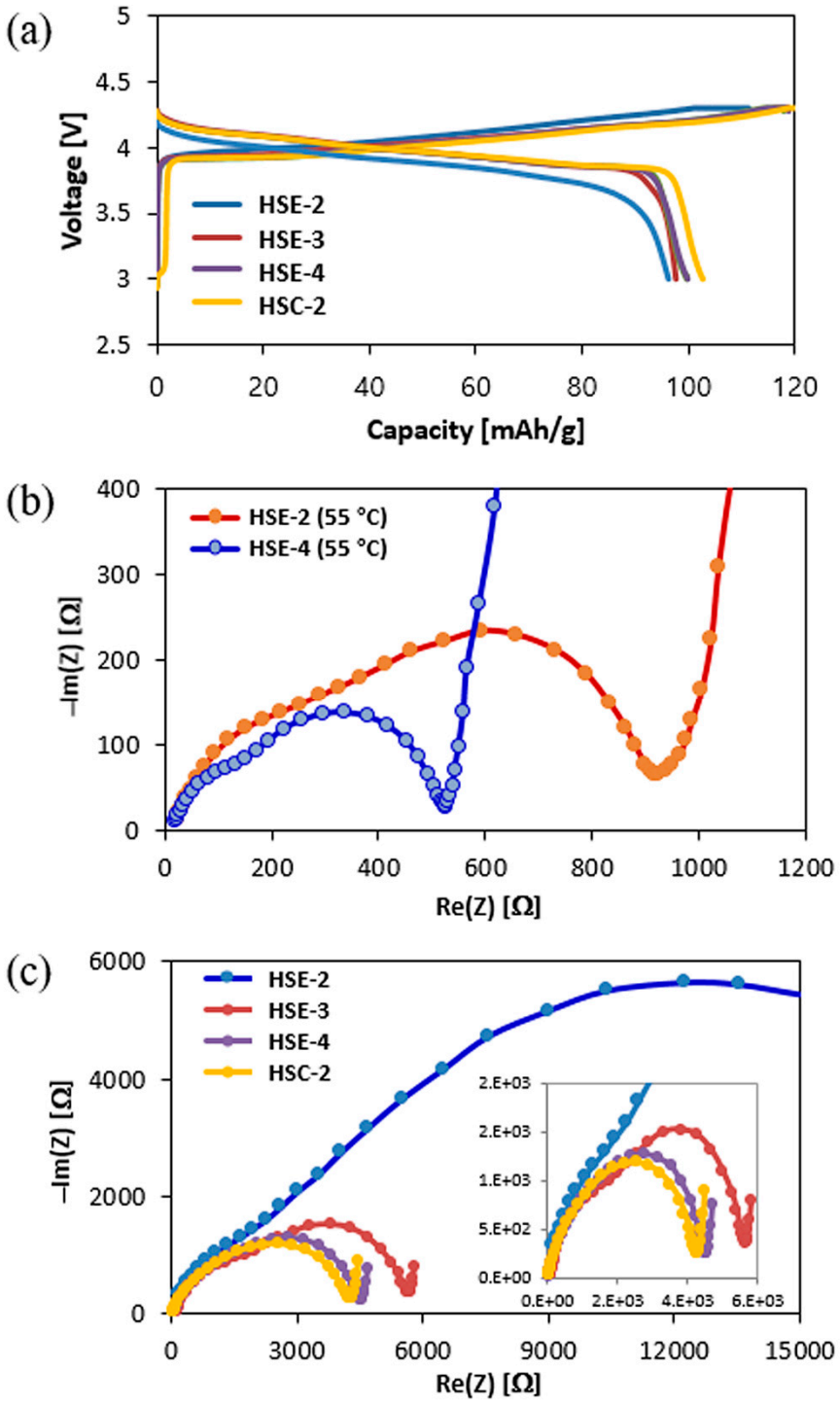

Preprints (www.preprints.org) | NOT PEER-REVIEWED | Posted: 7 August 2018 doi:10.20944/preprints201808.0145.v1

Figure 7